

When are radiology reports useful for training medical image classifiers?

Herman Bergström^{*1}, Zhongqi Yue¹, and Fredrik D. Johansson¹

¹Department of Computer Science & Engineering,

Chalmers University of Technology and University of Gothenburg

Abstract

Medical images used to train machine learning models are often accompanied by radiology reports containing rich expert annotations. However, relying on these reports as inputs for clinical prediction requires the timely manual work of a trained radiologist. This raises a natural question: when can radiology reports be leveraged *during training* to improve image-only classification? Prior works are limited to evaluating pre-trained image representations by fine-tuning them to predict diagnostic labels, often extracted from reports, ignoring tasks with labels that are weakly associated with the text. To address this gap, we conduct a systematic study of how radiology reports can be used during both pre-training and fine-tuning, across diagnostic and prognostic tasks (e.g., 12-month readmission), and under varying training set sizes. Our findings reveal that: (1) Leveraging reports during pre-training is beneficial for downstream classification tasks where the label is well-represented in the text; however, pre-training through explicit image-text alignment can be detrimental in settings where it's not; (2) Fine-tuning with reports can lead to significant improvements and even have a larger impact than the pre-training method in certain settings. These results provide actionable insights into when and how to leverage privileged text data to train medical image classifiers while highlighting gaps in current research.

1 Introduction

Radiology reports containing key findings from medical images are routinely produced in clinical practice. These texts have recently received much attention within the machine learning literature (Bannur et al., 2024; Yang et al., 2023; Tanno et al., 2025), and have been shown to be predictive of various patient outcomes, such as hospital readmission (Huang et al., 2019), ICU mortality (Lin et al., 2021), and cancer progression (Batch et al., 2022). Requiring manually written reports for test-time predictions is undesirable if the same prediction could be made from the medical image itself, but the prevalence of reports in retrospective data makes them attractive to use during training. In particular, reports can be used to improve few-shot or small-sample training of medical image classifiers, either by i) incorporating them in a *pre-training* objective (Zhang et al., 2022), or ii) viewing them as privileged information (PI) when *fine-tuning* for a specific task (Vapnik and Vashist, 2009).

Prior work has almost exclusively focused on the potential role of reports in *pre-training* image encoders—either incorporating them as paired supervision through multimodal objectives (Huang et al., 2021a; Zhou et al., 2023), or omitting them in favor of self-supervised learning (Pérez-García et al., 2024; Zhou et al., 2021)—with evaluation performed via report-free fine-tuning on *diagnostic* classification tasks, where labels are often extracted from the reports themselves (Johnson et al., 2019; Irvin et al., 2019; Bustos et al., 2020). As a result, the roles of radiology reports in *fine-tuning* and their potential utility for tasks beyond diagnosis remain largely

^{*}Corresponding author: hermanb@chalmers.se

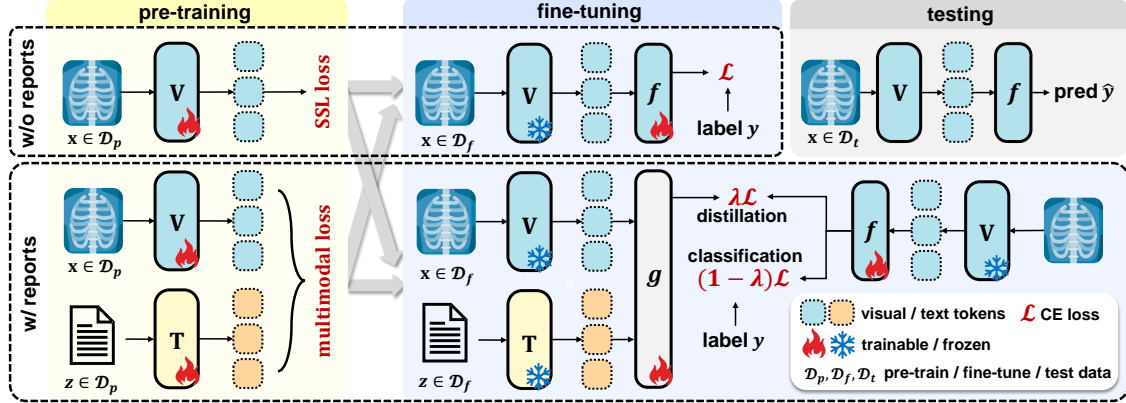


Figure 1: Training a medical image classifier with or without reports, divided into: pre-training and fine-tuning. Note that the classifier input is only a medical image at test time. V : visual encoder; T : text encoder; f : classifier; g : a privileged classifier using both image and report for prediction.

unexplored. For instance, pre-training with reports instead of relying on image-only self-supervision has been shown to yield representations that improve performance in diagnostic tasks (Zhang et al., 2022; Huang et al., 2021a). Yet it is unclear whether these results generalize to *prognostic* tasks—which aim to predict future clinical events (*e.g.*, 12-month readmission or 3-day discharge) that may not be explicitly captured in the original report—and intriguingly, whether incorporating reports during fine-tuning can compensate for the potential limitations of a self-supervised pre-trained representation or a small fine-tuning data set.

To address these gaps, we compile a benchmark that systematically investigates the usefulness of radiology reports for training medical image classifiers during both pre-training and fine-tuning. We summarize our paradigm in Figure 1. In the pre-training stage, we study six popular models that differ in both architecture (ResNet (He et al., 2016) vs. ViT (Dosovitskiy et al., 2021)), and learning objective, including self-supervised learning (Pérez-García et al., 2024; Zhou et al., 2020; Xiao et al., 2023), CLIP-style text-image alignment (Huang et al., 2021a; Bannur et al., 2023; Zhang et al., 2023), and masked image-text modeling (Zhou et al., 2023). For fine-tuning, we begin by highlighting that the relationships among the medical image (radiograph) X , report Z and label Y can vary significantly across diagnostic, prognostic, and other tasks, which in turn affects the utility of Z when training a classifier to predict Y from X . Motivated by this, we study a range of classification tasks with varying correlation and causality between Z and Y , and assess how using reports during fine-tuning by general distillation (Lopez-Paz et al., 2016) impacts performance in each setting. To the best of our knowledge, this is the first study of distillation from radiology reports, offering new insights into how privileged textual information can be transferred to image-only classifiers.

Our study leads to several interesting and novel findings: (1) Pre-training with report supervision is beneficial for diagnostic tasks at moderate sample sizes when the label is *strongly* correlated with the text. (2) Explicitly aligning image and text embeddings hurts downstream performance when the label is not captured well by the report, something that is more prominent for non-diagnostic prediction tasks. Crucially, we find that methods relying on text supervision *in addition to* self-supervision avoid this pitfall. (3) Incorporating reports during fine-tuning, even when they are not available at test time, can yield substantial gains in accuracy.

2 Method

Our goal is to study when training using radiology reports helps solve a C -way medical image-only classification task at test time, *i.e.*, predicting the label $y \in \{1, \dots, C\}$ from *only* a medical image x . We consider each training sample i in a data set \mathcal{D} as a triplet $(X = \mathbf{x}_i, Z = z_i, Y = y_i)$, where the image-label pair (\mathbf{x}_i, y_i) is additionally annotated with a radiology report z_i derived from \mathbf{x}_i to describe clinically significant observations. For brevity, we omit the subscript i when it is unnecessary to highlight the sample index. Training is divided into pre-training and fine-tuning. Next, we describe training procedures for both stages, with or without Z .

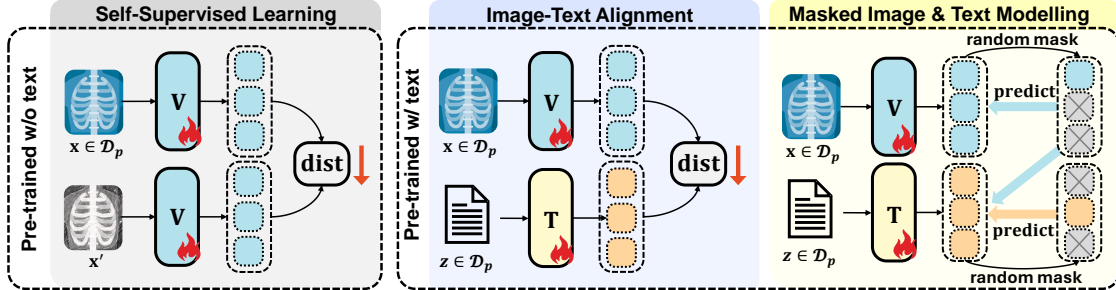


Figure 2: Three categories of pre-training objectives considered in this work, where \mathbf{x}' is an augmented view of \mathbf{x} , \mathcal{D}_p is the pre-training dataset, the fire symbol indicates trainable models, and dist denotes a distance function. V and T represent image (visual) and text encoders, respectively.

2.1 Pre-training with and without reports

In pre-training, we aim to learn a representation of images \mathbf{x} through a visual encoder V , which maps each \mathbf{x} into a sequence of visual tokens, *e.g.*, the patch embeddings in ViT (Dosovitskiy et al., 2021) or convolutional feature maps in ResNet (He et al., 2016). When medical reports are used in pre-training, analogously, we use a text encoder T , such as a BERT-style transformer, which maps each z into a sequence of text tokens. We consider 7 different models pre-trained for medical images from the literature, summarized in Table 1, illustrated in Figure 2, and described below.

Self-Supervised Learning RAD-DINO (Pérez-García et al., 2024), Medical MAE (Xiao et al., 2023), and C2L (Zhou et al., 2020) all leverage a self-supervised learning (SSL) objective without report supervision, which learns an image representation invariant to random augmentations. RAD-DINO and Medical MAE employ techniques such as masked image modeling (Oquab et al., 2023), while C2L uses a more classical contrastive learning approach.

Image-Text Alignment BioViL-T (Bannur et al., 2023), GLoRIA (Huang et al., 2021a) and BiomedCLIP (Zhang et al., 2023) use text supervision in a CLIP-style setup (Radford et al., 2021) by aligning image and text representation. In contrast to GLoRIA and BiomedCLIP, which use only a single image and its associated text as input, BioViL-T additionally includes previous radiographs to account for potential backward references in the report. We also note that the BiomedCLIP model has been trained on more general biomedical images; hence, radiographs and medical reports constitute a minor portion of its training set.

Masked Image & Text Modelling Lastly, we include MRM (Zhou et al., 2023), which is pre-trained with reports, but without explicit multi-modal alignment. Instead, given a subset of patches from an image, the model is trained to predict masked words in the report, as well as the remaining image patches. As such, its strategy combines image SSL and text supervision, encouraging the image representation to capture the contents of the report, while not being limited to it.

For the text encoder, we use the BERT model trained alongside BioViL-T in Bannur et al. (2023) as it has been fine-tuned to better capture disease progression. In Appendix C, we evaluate the impact of the choice of text model.

2.2 Fine-tuning

The goal during fine-tuning is to learn a classifier f that requires only image representations $V(\mathbf{x})$ as the input and outputs the softmax-normalized probabilities in \mathbb{R}^C for C -way classification. When fine-tuning *without reports*, this is simply achieved by standard supervised learning, optimizing the parameters of f to minimize the cross-entropy loss \mathcal{L} computed over each $(f(\mathbf{x}_i), y_i)$ in the training dataset. When fine-tuning

Table 1: An overview of the pre-trained models compared in this study. \blacklozenge indicates that the image and text representations have been explicitly aligned. Size refers to the input image resolution.

Model ($V(x)$)	Type	Size	Pre-Trained Using		Pre-Trained On		
			Image SSL	Text	MIMIC	CheXpert	Other
RAD-DINO	ViT-B/14	518	✓	✗	✓	✓	✓
C2L	ResNet-18	224	✓	✗	✓	✓	✓
Medical MAE	ViT-B/16	224	✓	✗	✓	✓	✓
MRM	ViT-B/16	224	✓	✓	✓	✗	✗
BioViL-T	ResNet-50	512	✗	✓ \blacklozenge	✓	✗	✗
GLoRIA	ResNet-50	224	✗	✓ \blacklozenge	✗	✓	✗
BiomedCLIP	ViT-B/16	224	✗	✓ \blacklozenge	✗	✗	✓

with reports, we adopt generalized distillation for privileged information (reports), as popularized by Lopez-Paz et al. (2016)—a two stage approach, described below.

In the first stage, we aim to learn a teacher model g that takes $V(\mathbf{x})$ and $T(z)$ as the input, and outputs the probabilities, analogous to f . The objective is given by:

$$\min_g \sum_{i=1}^N \left[\mathcal{L}\left(g(V(\mathbf{x}_i), T(z_i)), y_i\right) \right], \quad (1)$$

where N is the size of the training dataset. In the second stage, we train f as a student model by distilling from the teacher g according to the learning objective

$$\min_f \sum_{i=1}^N \left[(1 - \lambda) \mathcal{L}\left(f(V(\mathbf{x}_i)), y_i\right) + \lambda \mathcal{L}\left(f(V(\mathbf{x}_i)), g^\tau(V(\mathbf{x}_i), T(z_i))\right) \right], \quad (2)$$

where $\lambda \in [0, 1]$ is the imitation parameter that balances the importance of following the teacher prediction, and $g^\tau(\cdot)$ denotes the teacher prediction computed with a softmax temperature of $\tau > 0$.

Previous works have observed that results are rarely sensitive to λ (Yang et al., 2022b), and we found $\lambda = 0.75$ to work well in our experiments. In Appendix C we include the ablation of τ . Overall, this setup trains the image-only classifier f to imitate a privileged teacher g that has access to reports, thereby guiding f to classify \mathbf{x} like a radiologist without accessing z at test time. For direct comparison, we also implement a self-distillation baseline, which is trained without reports by distilling from an image-only teacher model.

Fine-tuning architecture. We design f to first perform self-attention on the visual tokens output from V , where the query, key and value networks are learnable linear heads. Then we perform mean pooling on the self-attention tokens output and feed the resulting feature into a learnable linear classifier. The teacher network g processes the text tokens output from T with a separate self-attention and mean pooling step. Then, the pooled visual and text features are concatenated as the input to a single linear classifier. We choose this design as it performs well empirically (comparisons in Appendix C), without over-complicating the fine-tuning stage.

3 Experimental Setup

Next, we detail and motivate the design choices behind our experiments aimed at aiding understanding of the benefits of using radiology reports in pre-training and fine-tuning of image-only classifiers.

3.1 The diversity of image classification tasks

The vast majority of work in medical image classification has focused on *diagnostic tasks*, where the label Y represents the presence of one or more medical conditions (Johnson et al., 2019; Bustos et al., 2020; Irvin

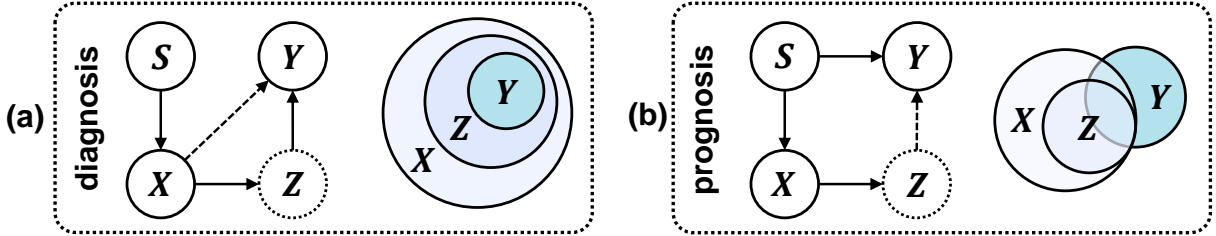


Figure 3: Example causal graphs under the (a) diagnosis or (b) prognosis setting, where S : (unobserved) patient state, X : medical image, Z : radiology report (potentially missing at test time) and Y : target label. Dashed edges indicate associations likely to be weak. The accompanying Venn diagrams conceptually illustrate the relationship between the information contained in the observed variables.

et al., 2019). This ignores that clinical prediction challenges frequently involve *prognostic* targets such as future (*e.g.*, 30-day) mortality (Nam et al., 2022), hospital readmission (Huang et al., 2019), and disease forecasting (Li et al., 2021). Critically, the causality and association strength between radiograph X , report Z , and target variable Y can vary substantially depending on the nature of the task. We illustrate this in Figure 3 and give examples below. In many *diagnostic* tasks, like pneumonia detection (Rajpurkar et al., 2017), the target label Y is determined almost completely by the radiology report Z (see Figure 3a). Often, the report will contain mentions of a likely diagnosis, and if not, it is written to aid physicians in making one. This is taken to its extreme in currently widely-used benchmarks where the label Y has been extracted from Z based on a set of hand-written rules (Bustos et al., 2020; Johnson et al., 2019; Irvin et al., 2019). In other words, Y is deterministically caused by Z . In contrast, *prognostic* tasks, such as predicting 3-day discharge or 12-month readmission (Kansagara et al., 2011), the target variable Y is often highly stochastic relative to both the image X and report Z (Figure 3b). Outcomes depend largely on latent disease progression and external factors, while radiographs and reports play only a limited, indirect role by informing treatment decisions.

Figure 3 does not represent all categories of medical image classification. Auxiliary tasks like predicting the age of a patient (Pérez-García et al., 2024) fit in neither the prognostic nor diagnostic category (we label them *auxiliary*), and their causal graphs are harder to determine. Yet, it is clear that the nature of the task affects how much information the report Z carries about Y , and whether it can be extracted from X . Consequently, *we need richer benchmarks to fully understand the effectiveness of utilizing reports in pre-training and fine-tuning of medical image classifiers*.

3.2 Benchmark and evaluation details

We compile our experiments from two existing datasets, MIMIC-CXR (Johnson et al., 2019) and INSPECT (Huang et al., 2023), as they both contain radiology reports. INSPECT is a multimodal dataset containing CT scans of patients at risk of pulmonary embolism. We reconstruct chest X-rays from these CT volumes using digital radiograph reconstruction¹. None of the image encoders have been trained on this dataset, so it offers a fair test of generalization. We refer to Appendix A for more information regarding this, preprocessing of images and reports, and dataset construction.

1) MIMIC-CXR, where we consider the following tasks:

- MIMIC 5x1200 - *Diagnostic* (6,000 images): We perform the common task of predicting diagnostic labels extracted from radiological reports. To do this, we construct MIMIC CXR 5x1200 (similar to CheXpert 5x200 in Huang et al. (2021a)) by choosing a subset of the MIMIC-CXR-JPG subjects that have had exactly one of five labels assigned to them. Following Irvin et al. (2019), these labels are Atelectasis, Cardiomegaly, Edema, Pleural Effusion, and Consolidation. The final dataset includes 1200 images per label (1000 for training and 200 for evaluation).
- Age - *Auxiliary* (35,242 images): To evaluate model performance on targets rarely discussed in the report, we predict the age of a patient based on their radiograph. We construct a classification problem by dividing

¹The code for this will be made available

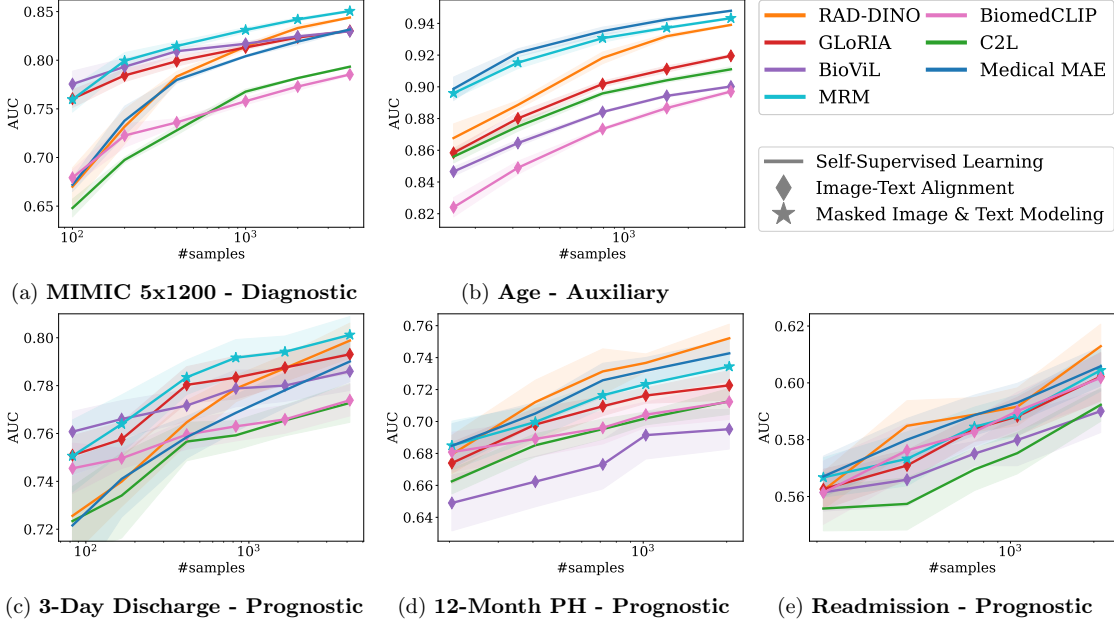


Figure 4: A comparison of the sample efficiency of different backbones. The plots are averaged over 5 seeds, except for Readmission, which is averaged over 10. The shaded area regions represent the 90% CI. The x-axis is on a logarithmic scale. AUPRC results are included in Appendix B

the ages into 5 bins, as done in Pérez-García et al. (2024). For each seed, 90% of images are sampled for training, with 10% withheld for validation.

- 3-Day Discharge - *Prognostic* (18,490 images): By linking the images in MIMIC-CXR to the patient records in MIMIC-IV (Johnson et al., 2023), we gain access to admission information for each patient. As a short-term prognostic target, we predict whether a patient will be discharged in the coming 3 days. For each seed, 90% of images are used for training, and 10% withheld for validation.

2) INSPECT, where we consider the following tasks:

- 12-Month PH - *Prognostic* (5,449 images): A binary classification task where 1 indicates that a patient was diagnosed with pulmonary hypertension (PH) within 12 months of an image being taken. The dataset is collected by removing the censored samples and then artificially balancing it by subsampling the number of patients that did not experience the event. For each seed, 75% of images are sampled for training, while 25% are withheld for validation.
- Readmission - *Prognostic* (5,651): A binary classification task, predicting whether a patient will be readmitted in the coming 12 months. Censored patients were removed, and the dataset was artificially balanced similar to 12-Month PH. For each seed, 75% of images are sampled for training, while 25% are withheld for validation.

We fine-tune the 6 models covered in Section 2 on each of these datasets. All models are trained with a learning rate of 10^{-4} using the Adam optimizer and a batch size of 64. Performance is evaluated by measuring AUC after every epoch, with one-versus-rest and micro averaging for the multiclass problems. When training the teacher model, we save the version with the highest AUC on the validation set. We used the distillation temperature parameter $\tau = 0.25$ for all datasets except MIMIC 5x1200, which used $\tau = 2.5$. Experiments are averaged over multiple seeds with different network parameter initializations and training subsets. More detailed information in Appendix A.

4 Related Work

Evaluation of medical image models is challenging due to differences in preprocessing, training, and validation datasets. Zhou et al. (2024) introduce BenchX to standardize evaluation of medical Vision Language Models (VLMs), but focus on pre-training representations and tasks like segmentation and report generation rather than comparing with self-supervised methods. Khader et al. (2023) show ICU survival prediction improves when combining chest X-rays with electronic health records, while Weissman et al. (2018) demonstrate gains from including clinical notes. Castro et al. (2020) emphasize the importance of understanding the causal relationship between medical images and their annotations and argue that there is often a mismatch between the training dataset and the target application.

Learning using privileged information allows models access to additional features during training but not at test time (Vapnik and Vashist, 2009). Generalized distillation was popularized by Lopez-Paz et al. (2016) and has been applied to recommendation systems using richer supervision (Yang et al., 2022b; Xu et al., 2020). Transfer and Marginalize (TRAM) (Collier et al., 2022) addresses noisy labels, with Ortiz-Jimenez et al. (2023) showing PI helps models avoid overfitting shortcuts. Other work uses intermediate steps in time-series as PI (Jung and Johansson, 2022; Karlsson et al., 2022), improving sample efficiency by learning transformations between them.

Table 2: A comparison of text-only and image-only models. Text results come from fine-tuning the BioViL-T BERT model, "Image AUC" corresponds to the best-performing model.

Dataset	M 5x1200	Age	3-Day	12-Month PH	Readmission
Fraction	5%	1%	1%	5%	5%
Text AUC (sd)	96.4 (0.0)	78.5 (0.9)	72.5 (1.5)	71.0 (1.7)	57.4 (1.9)
Image AUC (sd)	79.9 (1.1)	92.1 (0.3)	77.4 (0.9)	68.5 (2.1)	56.7 (1.4)
Image Model	MRM	Medical MAE	BioViL	MRM	Medical MAE
Fraction	50%	10%	10%	50%	50%
Text AUC (sd)	98.5 (0.0)	80.6 (0.2)	76.0 (0.8)	76.6 (0.8)	60.7 (1.4)
Image AUC (sd)	84.2 (0.2)	94.8 (0.0)	79.4 (0.9)	75.2 (1.2)	61.3 (1.5)
Image Model	MRM	Medical MAE	MRM	RAD-DINO	RAD-DINO

5 Results

5.1 Impact of pre-training with reports

Recently, text-based supervision during pre-training has been criticized (Pérez-García et al., 2024) as explicit alignment has been shown to decrease the generality of visual representations (Zhai et al., 2022; Yang et al., 2022a). In Figure 4, we perform experiments to see if and when this is noticeable in the medical image classification setting. To gauge the predictiveness of the reports (i.e., how well we can predict Y from Z), we include Table 2, which compares a text-only model against the best-performing image-only model.

Explicitly aligning with reports limits generalizability. As expected (see Section 3.1), we observe the highest relative performance of GLoRIA and BioViL compared to other models in the **MIMIC 5x1200** experiment (Figure 4a), where the labels have been extracted from the reports. This is mainly evident in the low sample regime, and RAD-DINO overtakes both when the number of samples increases to over 1,000. However, when predicting **Age** (still using images from the MIMIC dataset), the relative performance of these algorithms decreases significantly compared to backbones pre-trained with self-supervision. Instead, Medical MAE, MRM, and RAD-DINO perform the best, with the previously poorly performing C2L achieving a higher AUC than BioViL, and only slightly lower than GLoRIA. The **Age** experiment has the largest gap

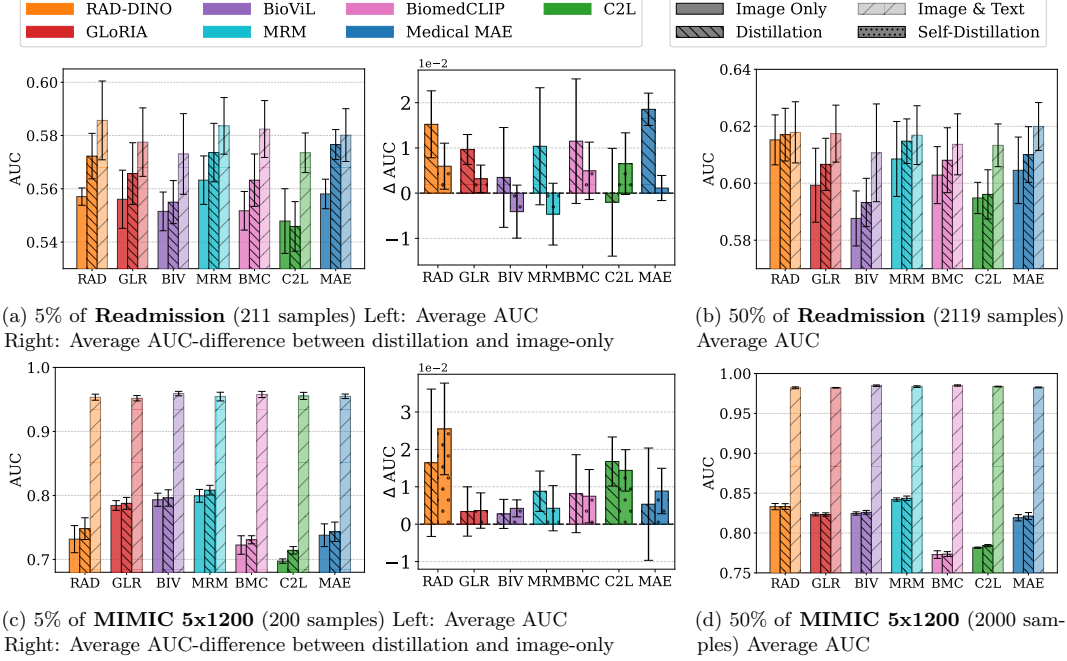


Figure 5: Distillation results on **Readmission** (prognostic) and **MIMIC 5x1200** (diagnostic) with different training sizes, averaged over 5 seeds. Bars represent the 95% CI. AUPRC results are found in Appendix B.

between image-only and text-only performance in Table 2, which offers a possible explanation as to why aligning with reports is not beneficial for this task. Finally, BiomedCLIP, which has been trained on more general biomedical images and their captions, performs poorly in both settings.

Image self-supervision is usually beneficial for prognostic tasks. For the prognostic tasks, the order of performance varies. In **3-Day Discharge** (Figure 4c), GLoRIA, BioViL, and MRM (all pre-trained with text supervision) perform well in the low sample regime. Yet, in the **12-Month PH** experiment (Figure 4d), GLoRIA and BioViL do not see the same benefits, with BioViL performing the worst in all sample sizes. The trend is similar in **Readmission** (Figure 4e). We hypothesize that while these tasks are prognostic, whether or not a patient is discharged in the coming days may be more closely correlated to a diagnostic label discussed in the radiology reports. For example, it is well possible for pneumothorax (one of the labels extracted from reports in MIMIC-CXR (Johnson et al., 2019)) to persist for more than 3 days (Thachuthara-George, 2021). Lastly, the high sample efficiency of MRM in all experiments highlights the benefit of not explicitly aligning representations with text, but using text supervision as a complement to image self-supervision.

5.2 Fine-tuning with reports

Leveraging radiology reports during pre-training as a means to achieve better data efficiency has been widely studied (Zhang et al., 2022; Huang et al., 2021a; Bannur et al., 2023). At the same time, the use of these texts during fine-tuning has been ignored, leaving their possible usefulness for this unknown. We perform experiments on **MIMIC 5x1200**, **3-Day Discharge**, and **Readmission** (Figures 5 and 6) to explore whether distilling from a teacher with access to text can have a similar impact. Due to space constraints, results for **Age** and **12-Month PH** are provided in Appendix B.

Distillation can have a larger impact than pre-training. Interestingly, pre-training does not always have the largest effect on performance. In Figure 5a, distillation has a higher impact on the AUC than the choice of pre-training method when predicting **12-Month Readmission** in the small-sample domain. The

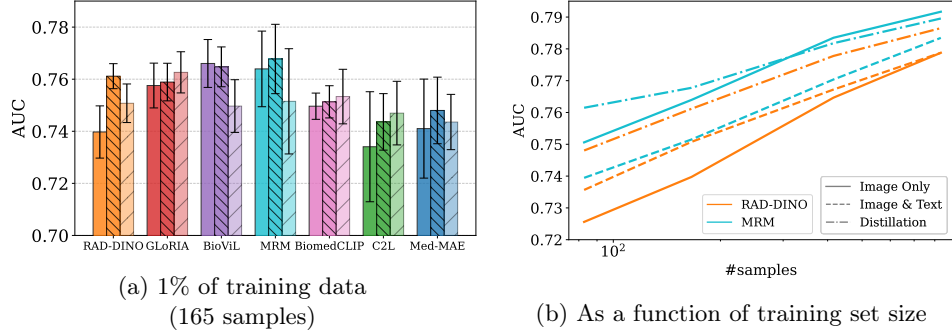


Figure 6: Mean AUC, averaged over 5 seeds, when performing distillation on **3-Day Discharge**.

results show that distillation from a teacher with access to the text report consistently increases the AUC across seeds, something that is not observed when applying self-distillation from an image-only model. As the number of samples grows (Figure 5b), distillation still leads to a meaningful performance increase, but the gap between different image backbones widens.

Distillation works poorly if the text is too predictive. On the other hand, the results of distillation on the **MIMIC 5x1200** dataset (Figures 5(c-d)) highlight that a strong multi-modal teacher does not imply that the student will benefit from distillation. The student sees no more benefit in distilling from the significantly more accurate teacher as opposed to performing self-distillation (Figure 5c). This aligns with previous research, which has observed that utilizing PI through distillation performs poorly if the information is too predictive of the label (Yang et al., 2022b; Ortiz-Jimenez et al., 2023). The results indicate that this is the case for diagnostic labels of this kind, further underscoring that the benefit from using reports for pre-training as opposed to generalized distillation depends on the task structure (as hypothesized in Section 3.1). The high performance of models pre-trained with text in Figure 4a brings into question whether an alternate fine-tuning method might better leverage reports in this setting, allowing self-supervised models to catch up.

Benefits of distillation are dependent on both task and backbone. We don't always benefit from applying distillation, even in the prognostic setting. Beyond variance with the task, our results show that not all encoders benefit the same when fine-tuning with PI. Medical MAE, RAD-DINO, MRM and GLoRIA see large performance increases in the **12-Month Readmission** experiment (Figure 5a), while BioViL and C2L do not improve. Similarly, RAD-DINO benefits more than any other model in the **3-Day Discharge** setting (Figure 6), and GLoRIA does not seem to benefit at all in contrast to before. The benefits are expected to depend on the relation between image (X), text (Z), and label (Y). In practice, we have both the image and text backbones frozen, meaning that the performance will depend on the relation between $V(x)$ and $T(z)$.

An image-only student can outperform a privileged teacher. Lastly, the multi-modal teacher can perform worse than the image-only baseline without access to the report (Figure 6a) in the low sample regime. This is possibly a result of the increase in the number of features and model complexity (introduced by the addition of a new modality), which can decrease performance in low-sample settings (Huang et al., 2021b). Despite this, in the **3-Day Discharge** experiment, we observe that the student can outperform the teacher it is distilling from (Figure 6b). While this may be surprising in the PI setting, a student network outperforming its teacher has been observed numerous times in literature (Furlanello et al., 2018; Pareek et al., 2024; Yang et al., 2022b) and forms the foundation of self-distillation. In Appendix B, we show results for each seed, demonstrating that RAD-DINO consistently outperforms the multi-modal model with distillation.

6 Conclusion

We have studied the utility of radiology reports in the pre-training and fine-tuning of medical image-only classifiers. To address the narrow focus of current classification benchmarks on diagnostic targets, we compiled a collection of diagnostic, prognostic, and auxiliary tasks. We compared the performance of 6 image encoders, pre-trained with or without radiology reports when fine-tuned for 5 image-only classification tasks, with or without reports during fine-tuning. Our results underscore the importance of task-diversity in evaluation to better understand the pros and cons of different methods. We find that 1) Pre-training with text shows the greatest benefit for diagnostic labels, but that 2) explicit text-alignment during pre-training can lose information about targets weakly associated with reports. Further, 3) fine-tuning with distillation from image-report models can have impact comparable to the choice of image encoder, but benefits depend on the encoder and task.

Our study is limited to using text as PI during fine-tuning with a single text encoder and a single learning objective (distillation). While our goal is to highlight the potential of leveraging radiology reports during fine-tuning, rather than identifying the best possible PI method, the fact that distillation does not improve performance even when the text is completely predictive (MIMIC 5x1200) indicates that future work may benefit from developing more refined approaches.

Acknowledgements

We thank Ida Häggström for her advice regarding digital radiograph reconstruction and for suggesting the Plastimatch software suite. We would also like to thank Victor Wählstrand Skärström for his input and valuable discussion at the start of this project. FDJ and HB are supported by Swedish Research Council Grant 2022-04748. FDJ is also supported in part by the Wallenberg AI, Autonomous Systems and Software Program, founded by the Knut and Alice Wallenberg Foundation. YZ is funded by the Wallenberg-NTU Presidential Postdoctoral Fellowship. The computations were enabled by resources provided by the National Academic Infrastructure for Supercomputing in Sweden (NAIIS), partially funded by the Swedish Research Council through grant agreement no. 2022-06725.

References

Emily Alsentzer, John R Murphy, Willie Boag, Wei-Hung Weng, Di Jin, Tristan Naumann, and Matthew McDermott. Publicly available clinical bert embeddings. *arXiv preprint arXiv:1904.03323*, 2019.

Shruthi Bannur, Stephanie Hyland, Qianchu Liu, Fernando Pérez-García, Maximilian Ilse, Daniel C. Castro, Benedikt Boecking, Harshita Sharma, Kenza Bouzid, Anja Thieme, Anton Schwaighofer, Maria Wetscherek, Matthew P. Lungren, Aditya Nori, Javier Alvarez-Valle, and Ozan Oktay. Learning To Exploit Temporal Structure for Biomedical Vision-Language Processing. pages 15016–15027, 2023.

Shruthi Bannur, Kenza Bouzid, Daniel C Castro, Anton Schwaighofer, Anja Thieme, Sam Bond-Taylor, Maximilian Ilse, Fernando Pérez-García, Valentina Salvatelli, Harshita Sharma, et al. Maira-2: Grounded radiology report generation. *arXiv preprint arXiv:2406.04449*, 2024.

Karen E Batch, Jianwei Yue, Alex Darcovich, Kaelan Lupton, Corinne C Liu, David P Woodlock, Mohammad Ali K El Amine, Pamela I Causa-Andrieu, Lior Gazit, Gary H Nguyen, et al. Developing a cancer digital twin: supervised metastases detection from consecutive structured radiology reports. *Frontiers in artificial intelligence*, 5:826402, 2022.

Benedikt Boecking, Naoto Usuyama, Shruthi Bannur, Daniel C Castro, Anton Schwaighofer, Stephanie Hyland, Maria Wetscherek, Tristan Naumann, Aditya Nori, Javier Alvarez-Valle, et al. Making the most of text semantics to improve biomedical vision-language processing. In *European conference on computer vision*, pages 1–21. Springer, 2022.

G. Bradski. The OpenCV Library. *Dr. Dobb's Journal of Software Tools*, 2000.

Aurelia Bustos, Antonio Pertusa, Jose-Maria Salinas, and Maria De La Iglesia-Vaya. Padchest: A large chest x-ray image dataset with multi-label annotated reports. *Medical image analysis*, 66:101797, 2020.

Daniel C Castro, Ian Walker, and Ben Glocker. Causality matters in medical imaging. *Nature Communications*, 11(1):3673, 2020.

Mark Collier, Rodolphe Jenatton, Effrosyni Kokopoulou, and Jesse Berent. Transfer and marginalize: Explaining away label noise with privileged information. In *International Conference on Machine Learning*, pages 4219–4237. PMLR, 2022.

Alexey Dosovitskiy, Lucas Beyer, Alexander Kolesnikov, Dirk Weissenborn, Xiaohua Zhai, Thomas Unterthiner, Mostafa Dehghani, Matthias Minderer, Georg Heigold, Sylvain Gelly, Jakob Uszkoreit, and Neil Houlsby. An Image is Worth 16x16 Words: Transformers for Image Recognition at Scale, June 2021. arXiv:2010.11929 [cs].

Tommaso Furlanello, Zachary Lipton, Michael Tschannen, Laurent Itti, and Anima Anandkumar. Born again neural networks. In *International conference on machine learning*, pages 1607–1616. PMLR, 2018.

Kaiming He, Xiangyu Zhang, Shaoqing Ren, and Jian Sun. Deep residual learning for image recognition. In *Proceedings of the IEEE conference on computer vision and pattern recognition*, pages 770–778, 2016.

Kexin Huang, Jaan Altosaar, and Rajesh Ranganath. Clinicalbert: Modeling clinical notes and predicting hospital readmission. *arXiv preprint arXiv:1904.05342*, 2019.

Shih-Cheng Huang, Liyue Shen, Matthew P. Lungren, and Serena Yeung. GLoRIA: A Multimodal Global-Local Representation Learning Framework for Label-Efficient Medical Image Recognition. pages 3942–3951, 2021a.

Shih-Cheng Huang, Zepeng Huo, Ethan Steinberg, Chia-Chun Chiang, Matthew P Lungren, Curtis P Langlotz, Serena Yeung, Nigam H Shah, and Jason A Fries. Inspect: a multimodal dataset for pulmonary embolism diagnosis and prognosis. *arXiv preprint arXiv:2311.10798*, 2023.

Yu Huang, Chenzhuang Du, Zihui Xue, Xuanyao Chen, Hang Zhao, and Longbo Huang. What makes multi-modal learning better than single (provably). *Advances in Neural Information Processing Systems*, 34:10944–10956, 2021b.

Jeremy Irvin, Pranav Rajpurkar, Michael Ko, Yifan Yu, Silviana Ciurea-Illcus, Chris Chute, Henrik Marklund, Behzad Haghgoo, Robyn Ball, Katie Shpanskaya, et al. CheXpert: A large chest radiograph dataset with uncertainty labels and expert comparison. In *Proceedings of the AAAI conference on artificial intelligence*, volume 33, pages 590–597, 2019.

Alistair EW Johnson, Tom J Pollard, Nathaniel R Greenbaum, Matthew P Lungren, Chih-ying Deng, Yifan Peng, Zhiyong Lu, Roger G Mark, Seth J Berkowitz, and Steven Horng. Mimic-cxr-jpg, a large publicly available database of labeled chest radiographs. *arXiv preprint arXiv:1901.07042*, 2019.

Alistair EW Johnson, Lucas Bulgarelli, Lu Shen, Alvin Gayles, Ayad Shammout, Steven Horng, Tom J Pollard, Sicheng Hao, Benjamin Moody, Brian Gow, et al. Mimic-iv, a freely accessible electronic health record dataset. *Scientific data*, 10(1):1, 2023.

Bastian Jung and Fredrik D Johansson. Efficient learning of nonlinear prediction models with time-series privileged information. *Advances in Neural Information Processing Systems*, 35:19048–19060, 2022.

Devan Kansagara, Honora Englander, Amanda Salanitro, David Kagen, Cecelia Theobald, Michele Freeman, and Sunil Kripalani. Risk prediction models for hospital readmission: a systematic review. *Jama*, 306(15):1688–1698, 2011.

Rickard KA Karlsson, Martin Willbo, Zeshan M Hussain, Rahul G Krishnan, David Sontag, and Fredrik Johansson. Using time-series privileged information for provably efficient learning of prediction models. In *International Conference on Artificial Intelligence and Statistics*, pages 5459–5484. PMLR, 2022.

Firas Khader, Jakob Nikolas Kather, Gustav Müller-Franzes, Tianci Wang, Tianyu Han, Soroosh Tayebi Arasteh, Karim Hamesch, Keno Bressem, Christoph Haarburger, Johannes Stegmaier, et al. Medical transformer for multimodal survival prediction in intensive care: integration of imaging and non-imaging data. *Scientific Reports*, 13(1):10666, 2023.

Jing Li, Botong Wu, Xinwei Sun, and Yizhou Wang. Causal Hidden Markov Model for Time Series Disease Forecasting. pages 12105–12114, 2021.

Mingquan Lin, Song Wang, Ying Ding, Lihui Zhao, Fei Wang, and Yifan Peng. An empirical study of using radiology reports and images to improve icu-mortality prediction. In *2021 IEEE 9th International Conference on Healthcare Informatics (ICHI)*, pages 497–498. IEEE, 2021.

David Lopez-Paz, Léon Bottou, Bernhard Schölkopf, and Vladimir Vapnik. Unifying distillation and privileged information, February 2016. arXiv:1511.03643 [cs, stat].

Ju Gang Nam, Hye-Rin Kang, Sang Min Lee, Hyungjin Kim, Chanyoung Rhee, Jin Mo Goo, Yeon-Mok Oh, Chang-Hoon Lee, and Chang Min Park. Deep learning prediction of survival in patients with chronic obstructive pulmonary disease using chest radiographs. *Radiology*, 305(1):199–208, 2022.

Maxime Oquab, Timothée Darcet, Théo Moutakanni, Huy Vo, Marc Szafraniec, Vasil Khalidov, Pierre Fernandez, Daniel Haziza, Francisco Massa, Alaaeldin El-Nouby, et al. Dinov2: Learning robust visual features without supervision. *arXiv preprint arXiv:2304.07193*, 2023.

Guillermo Ortiz-Jimenez, Mark Collier, Anant Nawalgaria, Alexander Nicholas D’Amour, Jesse Berent, Rodolphe Jenatton, and Efi Kokopoulou. When does privileged information explain away label noise? In *International Conference on Machine Learning*, pages 26646–26669. PMLR, 2023.

Divyansh Pareek, Simon S Du, and Sewoong Oh. Understanding the gains from repeated self-distillation. *Advances in Neural Information Processing Systems*, 37:7759–7796, 2024.

Fernando Pérez-García, Harshita Sharma, Sam Bond-Taylor, Kenza Bouzid, Valentina Salvatelli, Maximilian Ilse, Shruthi Bannur, Daniel C Castro, Anton Schwaighofer, Matthew P Lungren, et al. Rad-dino: Exploring scalable medical image encoders beyond text supervision. *arXiv preprint arXiv:2401.10815*, 2024.

Alec Radford, Jong Wook Kim, Chris Hallacy, Aditya Ramesh, Gabriel Goh, Sandhini Agarwal, Girish Sastry, Amanda Askell, Pamela Mishkin, Jack Clark, et al. Learning transferable visual models from natural language supervision. In *International conference on machine learning*, pages 8748–8763. PmLR, 2021.

Pranav Rajpurkar, Jeremy Irvin, Kaylie Zhu, Brandon Yang, Hershel Mehta, Tony Duan, Daisy Ding, Aarti Bagul, Curtis Langlotz, Katie Shpanskaya, et al. Chexnet: Radiologist-level pneumonia detection on chest x-rays with deep learning. *arXiv preprint arXiv:1711.05225*, 2017.

Gregory C Sharp, Rui Li, John Wolfgang, G Chen, Marta Peroni, Maria Francesca Spadea, Shinichro Mori, Junan Zhang, James Shackleford, and Nagarajan Kandasamy. Plastimatch: an open source software suite for radiotherapy image processing. In *Proceedings of the XVI’th International Conference on the use of Computers in Radiotherapy (ICCR), Amsterdam, Netherlands*, volume 3, 2010.

Ryutaro Tanno, David GT Barrett, Andrew Sellergren, Sumedh Ghaisas, Sumanth Dathathri, Abigail See, Johannes Welbl, Charles Lau, Tao Tu, Shekoofeh Azizi, et al. Collaboration between clinicians and vision–language models in radiology report generation. *Nature Medicine*, 31(2):599–608, 2025.

Joseph Thachuthara-George. Pneumothorax in patients with respiratory failure in icu. *Journal of thoracic disease*, 13(8):5195, 2021.

Vladimir Vapnik and Akshay Vashist. A new learning paradigm: Learning using privileged information. *Neural networks*, 22(5-6):544–557, 2009.

Gary E Weissman, Rebecca A Hubbard, Lyle H Ungar, Michael O Harhay, Casey S Greene, Blanca E Himes, and Scott D Halpern. Inclusion of unstructured clinical text improves early prediction of death or prolonged icu stay. *Critical care medicine*, 46(7):1125–1132, 2018.

Junfei Xiao, Yutong Bai, Alan Yuille, and Zongwei Zhou. Delying into masked autoencoders for multi-label thorax disease classification. In *Proceedings of the IEEE/CVF Winter Conference on Applications of Computer Vision*, pages 3588–3600, 2023.

Chen Xu, Quan Li, Junfeng Ge, Jinyang Gao, Xiaoyong Yang, Changhua Pei, Fei Sun, Jian Wu, Hanxiao Sun, and Wenwu Ou. Privileged features distillation at taobao recommendations. In *Proceedings of the 26th ACM SIGKDD International Conference on Knowledge Discovery & Data Mining*, pages 2590–2598, 2020.

Jinyu Yang, Jiali Duan, Son Tran, Yi Xu, Sampath Chanda, Liqun Chen, Belinda Zeng, Trishul Chilimbi, and Junzhou Huang. Vision-language pre-training with triple contrastive learning. In *Proceedings of the IEEE/CVF Conference on Computer Vision and Pattern Recognition*, pages 15671–15680, 2022a.

Shuo Yang, Sujay Sanghavi, Holakou Rahamanian, Jan Bakus, and Vishwanathan SVN. Toward understanding privileged features distillation in learning-to-rank. *Advances in Neural Information Processing Systems*, 35: 26658–26670, 2022b.

Shuxin Yang, Xian Wu, Shen Ge, Zhuozhao Zheng, S Kevin Zhou, and Li Xiao. Radiology report generation with a learned knowledge base and multi-modal alignment. *Medical Image Analysis*, 86:102798, 2023.

Xiaohua Zhai, Xiao Wang, Basil Mustafa, Andreas Steiner, Daniel Keysers, Alexander Kolesnikov, and Lucas Beyer. Lit: Zero-shot transfer with locked-image text tuning. In *Proceedings of the IEEE/CVF conference on computer vision and pattern recognition*, pages 18123–18133, 2022.

Sheng Zhang, Yanbo Xu, Naoto Usuyama, Hanwen Xu, Jaspreet Bagga, Robert Tinn, Sam Preston, Rajesh Rao, Mu Wei, Naveen Valluri, et al. Biomedclip: a multimodal biomedical foundation model pretrained from fifteen million scientific image-text pairs. *arXiv preprint arXiv:2303.00915*, 2023.

Yuhao Zhang, Hang Jiang, Yasuhide Miura, Christopher D. Manning, and Curtis P. Langlotz. Contrastive Learning of Medical Visual Representations from Paired Images and Text. In *Proceedings of the 7th Machine Learning for Healthcare Conference*, pages 2–25. PMLR, December 2022. ISSN: 2640-3498.

Hong-Yu Zhou, Shuang Yu, Cheng Bian, Yifan Hu, Kai Ma, and Yefeng Zheng. Comparing to learn: Surpassing imagenet pretraining on radiographs by comparing image representations. In *Medical Image Computing and Computer Assisted Intervention–MICCAI 2020: 23rd International Conference, Lima, Peru, October 4–8, 2020, Proceedings, Part I* 23, pages 398–407. Springer, 2020.

Hong-Yu Zhou, Chenyu Lian, Liansheng Wang, and Yizhou Yu. Advancing radiograph representation learning with masked record modeling. *arXiv preprint arXiv:2301.13155*, 2023.

Yang Zhou, Tan Faith, Yanyu Xu, Sicong Leng, Xinxing Xu, Yong Liu, and Rick Siow Mong Goh. Benchx: A unified benchmark framework for medical vision-language pretraining on chest x-rays. *Advances in Neural Information Processing Systems*, 37:6625–6647, 2024.

Zongwei Zhou, Vatsal Sodha, Jiaxuan Pang, Michael B Gotway, and Jianming Liang. Models genesis. *Medical image analysis*, 67:101840, 2021.

Appendix

This appendix includes additional experimental results and information about the training setup. Further details about data processing, backbone model usage, and hyperparameters are presented in Section A. Section B contains the results from distillation experiments on **Age** and **12-Month PH**, and an additional diagnostic experiment on the **INSPECT** dataset that reaffirms the limited benefit of distillation when reports are too predictive. In Section C we perform multiple ablation experiments that motivate hyperparameter choices, while showcasing the robustness of our results. Sections D and E cover compute usage and dataset licenses, respectively.

A Training & Data Processing

When processing radiology reports in MIMIC-CXR we extract the impressions section and, if available, the findings section. **INSPECT** is a multimodal dataset containing CT images and pre-extracted impression sections from their accompanying reports. We perform digital radiograph reconstruction using the Plastimatch software suite (Sharp et al., 2010) to convert the CT volumes to (anterior-posterior) radiographs that our pre-trained backbones can process. After extracting the radiograph, we follow the preprocessing of Johnson et al. (2019) and apply histogram equalization using OpenCV (Bradski, 2000), before storing the images in the JPEG format with a 95 quality factor. The code used to process the **INSPECT** volumes will be made available.

Models collected from

- **RAD-DINO:** Model and weights fetched from huggingface.
- **GLoRIA:** Model collected from GitHub, weights from stanfordmedicine.app.box.com (ResNet-50).
- **BioViL:** Model and weights downloaded through the HI-ML Multimodal Toolbox Python package pypi.org/project/hi-ml-multimodal/.
- **MRM:** Acquired from <https://github.com/RL4M/MRM-pytorch>.
- **BiomedCLIP:** Model and weights fetched from huggingface.
- **C2L:** ResNet-18 weights downloaded from GitHub.
- **Medical MAE:** ViT-Base/16 weights (0.5M dataset) downloaded from GitHub.

Model-specific preprocessing Image preprocessing was chosen to match the preprocessing each backbone used during initial pre-training closely. All preprocessing not fetched from Huggingface was implemented using torchvision.

- **RAD-DINO:** The preprocessor was fetched from the corresponding huggingface repository.
- **GLoRIA & Medical MAE:** Resized such that the shorter side 238 pixels, followed by a 224×224 center crop. The pixel values were then rescaled to range $[0, 1]$, and the three channels subsequently normalized according to the ImageNet mean and standard deviation (mean= $[0.485, 0.456, 0.406]$ and std= $[0.229, 0.224, 0.225]$).
- **BioViL:** Images were initially resized such the shorter side was 512 pixels. 448×448 center-crop was applied followed by rescaling of values to range $[0, 1]$
- **MRM:** Derived from <https://github.com/RL4M/MRM-pytorch>. Resize to 224 pixels followed by 224×224 center crop. The image is converted to grayscale, rescaled to range $[0, 1]$ and normalized with mean=0.4978 and std=0.2449.

- **BiomedCLIP:** Fetched from [huggingface](#).
- **C2L:** Derived from GitHub. Image resize to 224 pixels followed by a 224×224 center-crop. Channels are rescaled to range $[0, 1]$ and normalized according to the ImageNet mean and std (provided previously).

For data augmentation, we used random resized crop between scales 0.4 and 0.9. During training, layer normalization was applied after extracting the pre-trained encoder features (*i.e.*, applied to $V(x)$ and/or $T(z)$). An additional normalization was used for the teacher model before concatenating the (self-attended and mean-pooled) image and text representations. Self-attention layers used a dropout layer ($p = 0.2$) on the attention weights before multiplying them with the value vector.

Training sizes and epochs Tables 3–7 cover the training dataset sizes, and their corresponding number of training epochs, used for the experiments in the main paper. Epochs were chosen such that all models had time to converge. We additionally plan to release the specific train-test splits for each seed.

Table 3: **MIMIC-CXR-JPG**

Fraction	#samples	Epochs
2.5%	100	100
5%	200	100
10%	400	100
25%	1000	50
50%	2000	50
100%	4000	50

Table 4: **Age**

Fraction	#samples	Epochs
1%	317	150
2.5%	792	100
5%	1585	100
10%	3171	50

Table 5: **3-Day Discharge**

Fraction	#samples	Epochs
0.5%	82	100
1%	165	100
2.5%	416	100
5%	829	50
10%	1662	50
25%	4145	50

Table 6: **Readmission**

Fraction	#samples	Epochs
5%	211	100
10%	423	100
17.5%	741	100
25%	1059	100
50%	2119	50

Table 7: **12-Month PH**

Fraction	#samples	Epochs
5%	204	100
10%	408	100
17.5%	715	100
25%	1022	100
50%	2044	50

Pre-training datasets Table 8 offers an overview of the datasets each model has been pre-trained with.

Table 8: An overview of the pre-training datasets of the models compared in this study.

Model	Pre-Trained On			
	MIMIC	CheXpert	NIH-CXR	Other
RAD-DINO	✓	✓	✓	✓
C2L	✓	✓	✓	✓
Medical MAE	✓	✓	✓	✗
MRM	✓	✗	✗	✗
BioViL-T	✓	✗	✗	✗
GLoRIA	✗	✓	✗	✗
BiomedCLIP	✗	✗	✗	✓

B Extended Results

B.1 AUPRC Figures

Figure 7 shows the AUPRC for the experiments in Figure 4. Micro-averaging was used for the multi-class tasks. We provide the AUPRC for the distillation experiments in Figure 8.

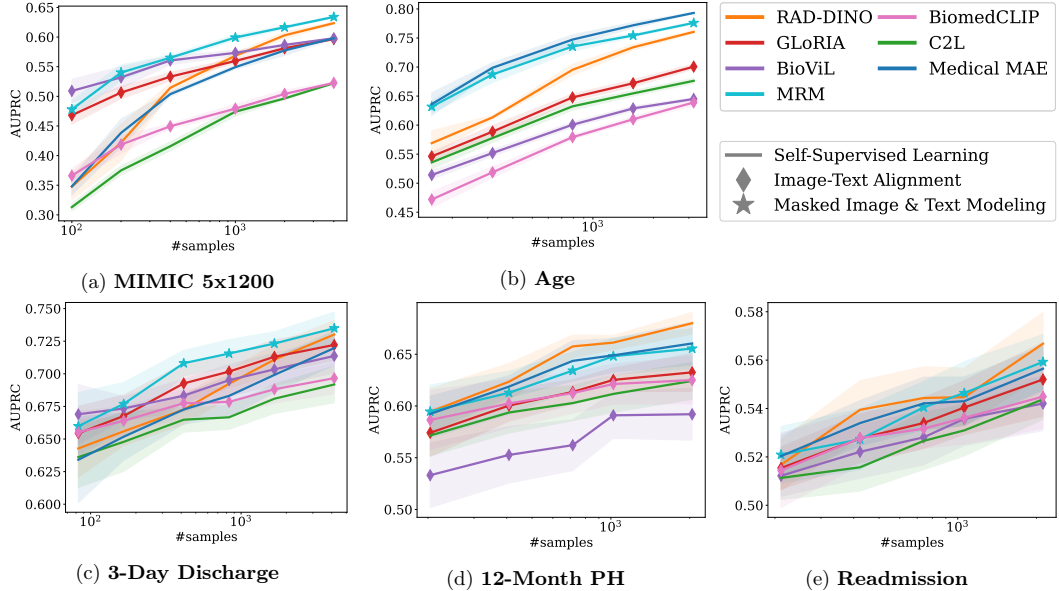


Figure 7: A comparison of the sample efficiency of different backbones. The plots are averaged over 5 seeds, except for Readmission, which is averaged over 10. The shaded area regions represent the 90% CI.

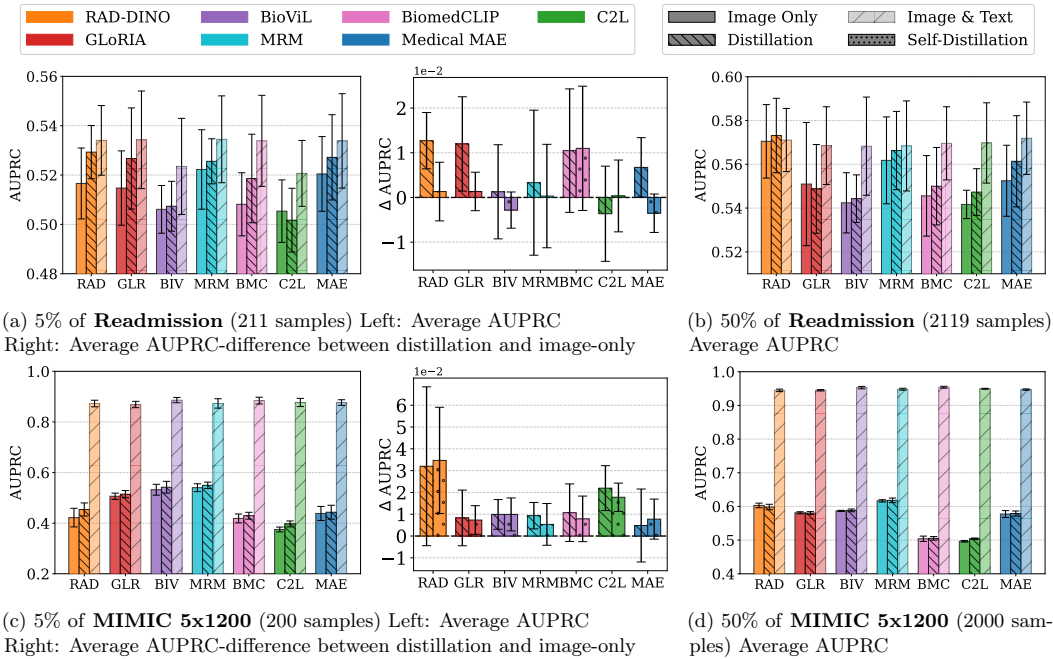


Figure 8: Distillation results on **Readmission** (prognostic) and **MIMIC 5x1200** (diagnostic) with different training set sizes, averaged over 5 seeds. Error bars represent the 95% confidence intervals.

B.2 Diagnostic Label INSPECT

We perform an additional experiment on the INSPECT dataset, in which models are trained to predict whether or not a patient currently suffers from **Pulmonary Embolism**. As before, this diagnostic label has been extracted from the accompanying radiology reports. Similar to **Readmission** and **12-Month PH**, we artificially balance the dataset by sub-sampling the number of negative labels to match the number of positive. The final dataset consists of 9,375 images, where 75% are designated for training and 25% for validation. The results (Figure 9) again indicate poor distillation performance when the text is too predictive of the label.

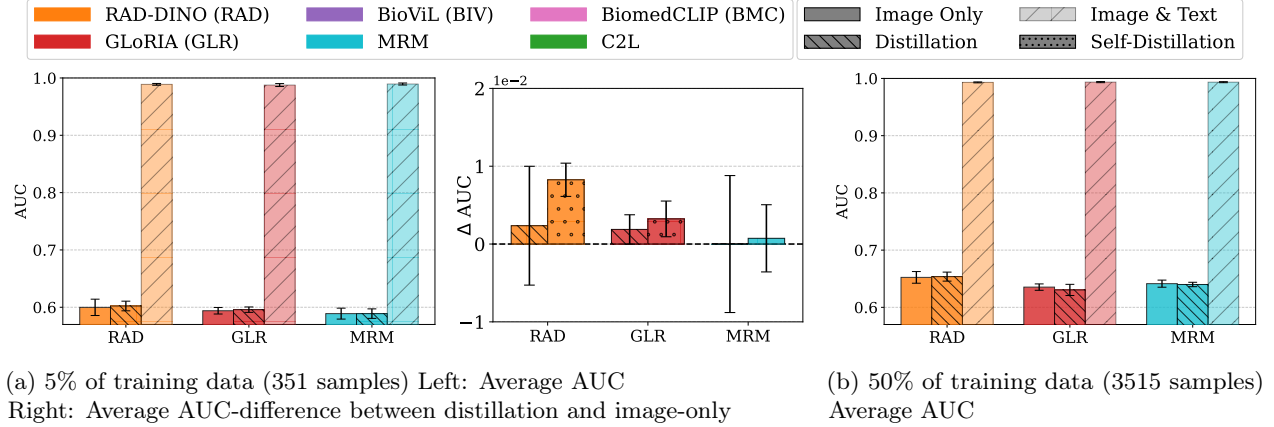


Figure 9: **Pulmonary Embolism**

B.3 Age and 12-Month PH results

We include the distillation results on the **12-Month PH** (Figure 10) and **Age** (Figure 11) datasets. Notably, in the Age experiment, the teacher performs worse on average for every backbone (even with more than 3,000 training samples), suggesting that the image is substantially more predictive than the radiology reports.

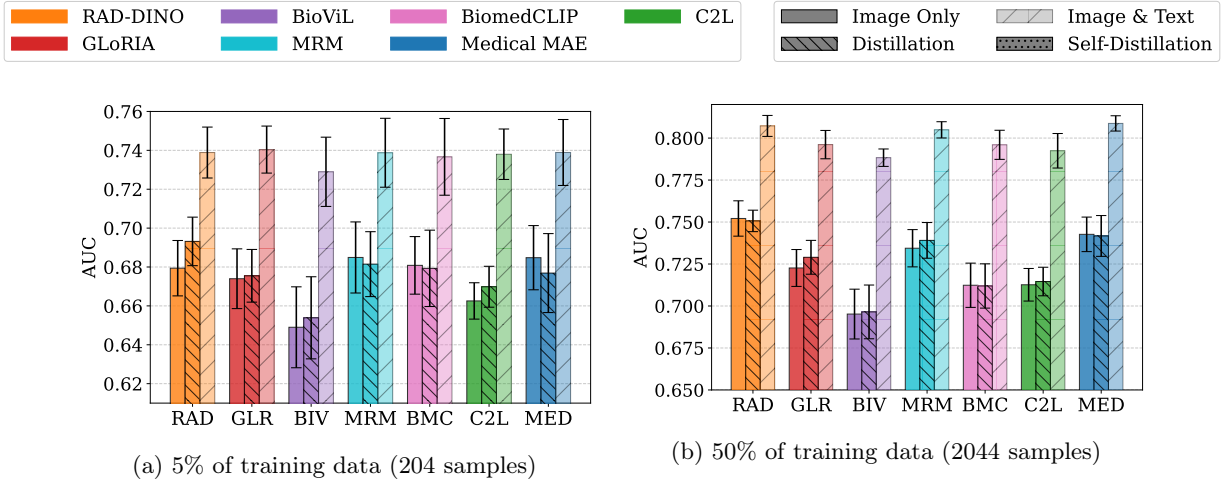


Figure 10: Mean AUC, averaged over 5 seeds, when performing distillation on **12-Month PH**.

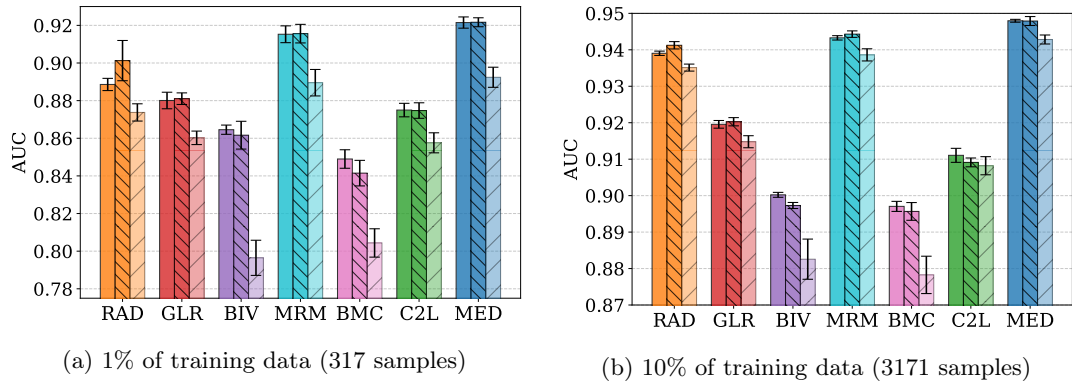


Figure 11: Mean AUC, averaged over 5 seeds, when performing distillation on **Age**.

B.4 Dino & MRM Seeds

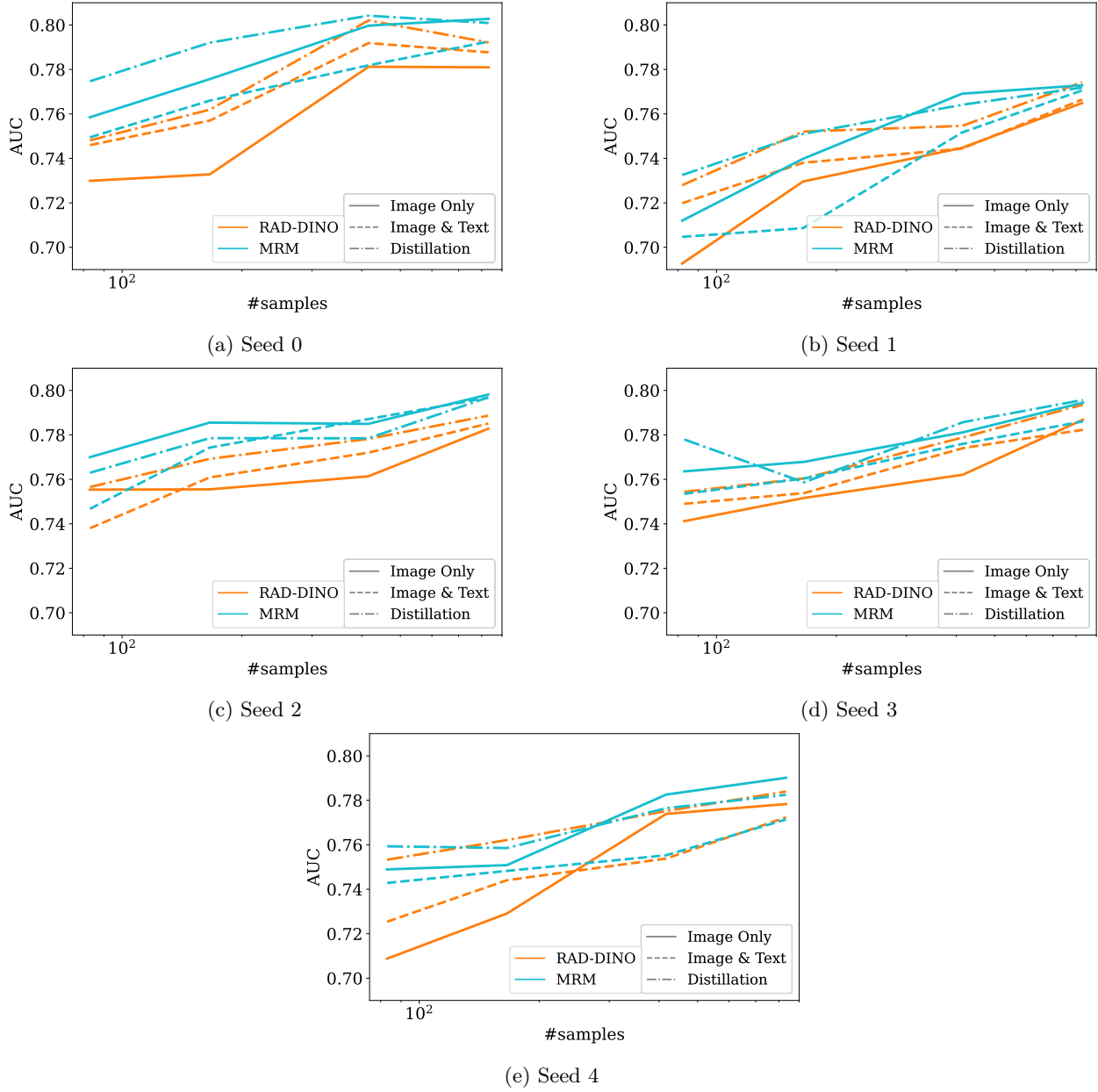


Figure 12: **3-Day Discharge** - RAD-DINO and MRM performance across the 5 seeds averaged in Figure 6b. In the case of RAD-DINO, the student consistently outperforms the teacher.

B.5 Readmission and MIMIC 5x1200 Seeds

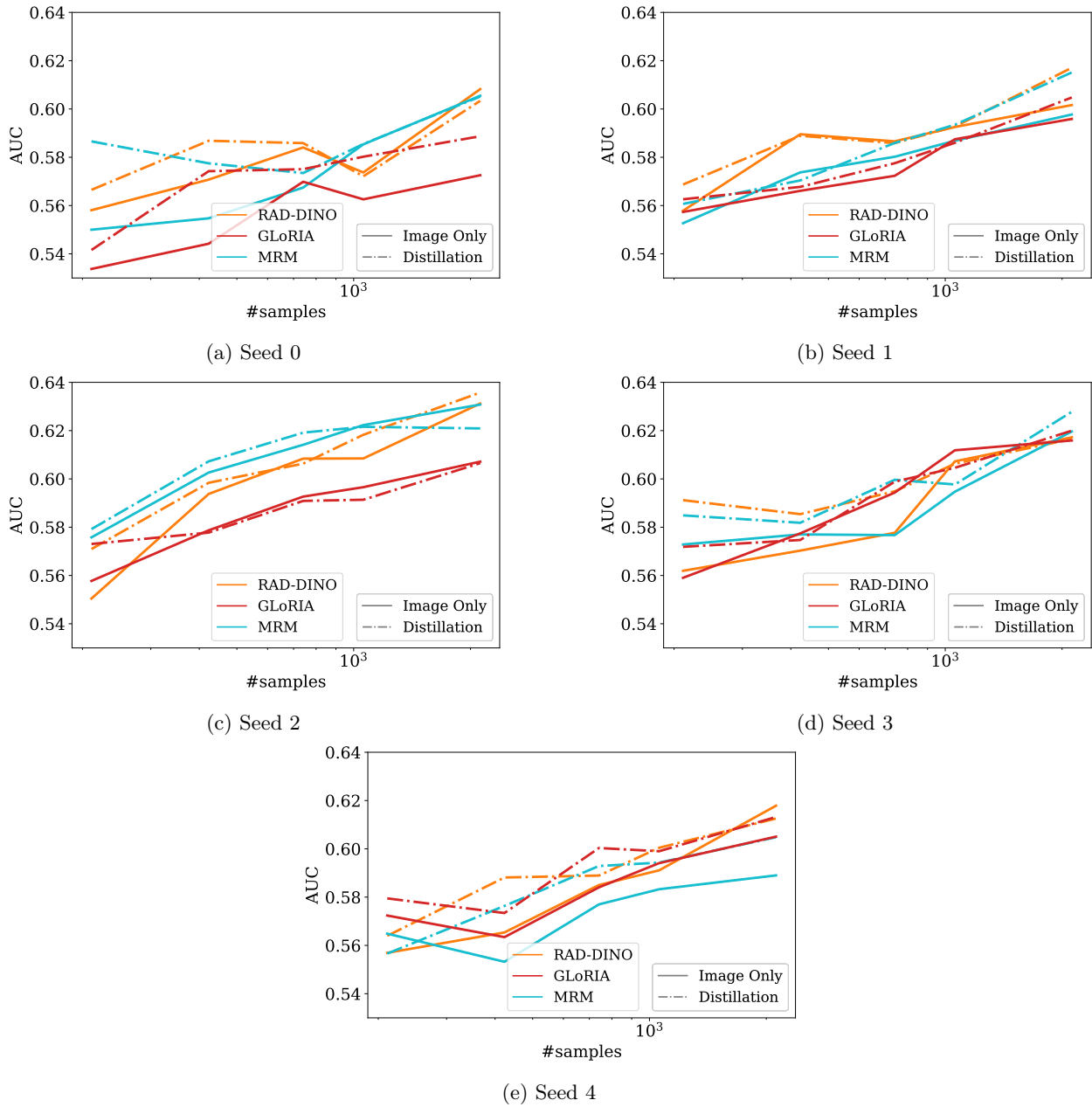


Figure 13: **Readmission** - A comparison of image-only models trained with and without distillation across the 5 seeds averaged in Figures 5a and 5b.

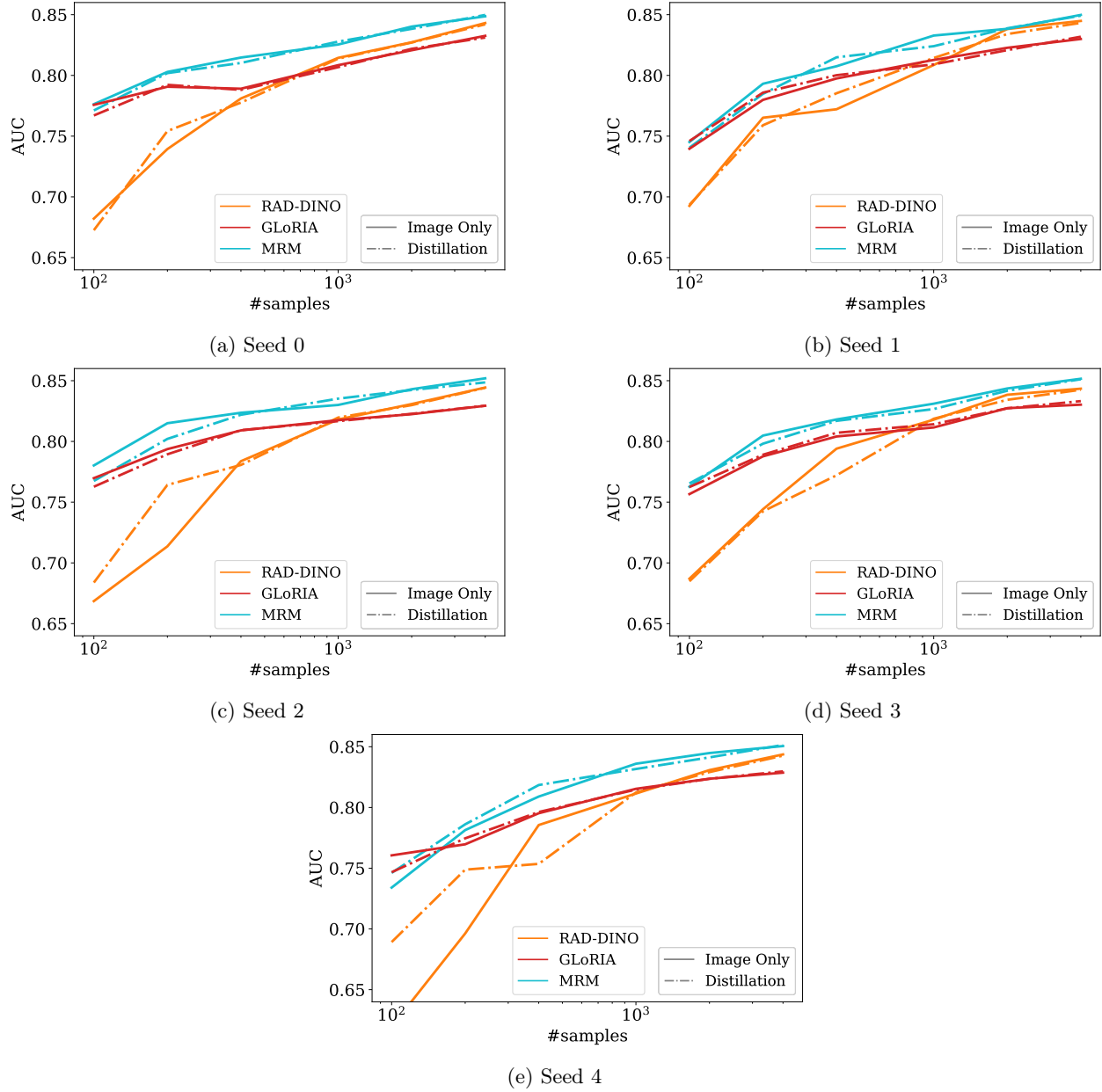


Figure 14: **MIMIC 5x1200** - A comparison of image-only models trained with and without distillation across the 5 seeds averaged in Figures 5c and 5d.

C Ablation experiments

C.1 Impact of Attention Head

Figures 15 and 16 demonstrate the impact of the fine-tuning head described in Section 2.2. "Attention Head" corresponds to the self-attention head used in all experiments in the main paper. For "Mean - LP", we have instead applied mean pooling over all local embeddings followed by linear probing. Lastly, we evaluated the performance using the RAD-DINO CLS token embedding instead of mean-pooling ("CLS - LP"). We used a learning rate of 10^{-3} when performing linear probing (mean- and cls-based). In these experiments, the self-attention head performs noticeably better as the number of samples increases, especially in the case of RAD-DINO. Furthermore, Figure 16 highlights the limitations of only using the CLS token.

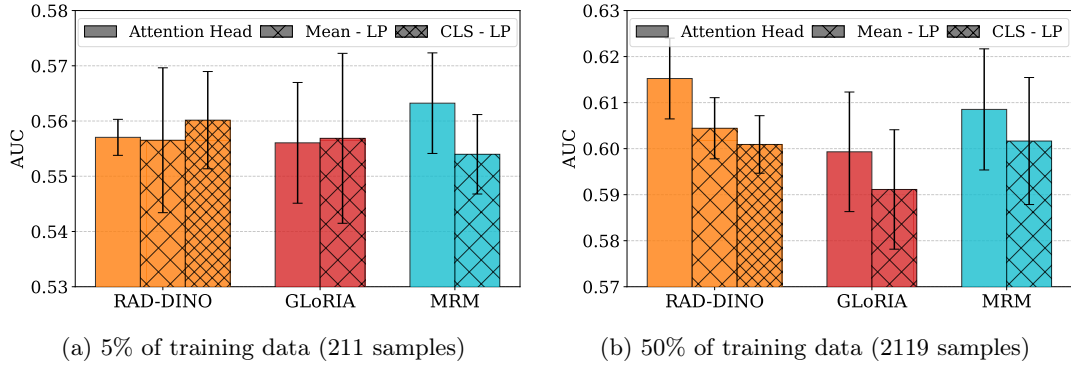


Figure 15: **Readmission** - Ablation of different fine-tuning heads on the image-only model. "Attention Head" is the self-attention head used in all experiments in the main paper, "Mean - LP" is mean-pooling followed by linear probing, and "CLS - LP" uses linear probing on the CLS token embedding.

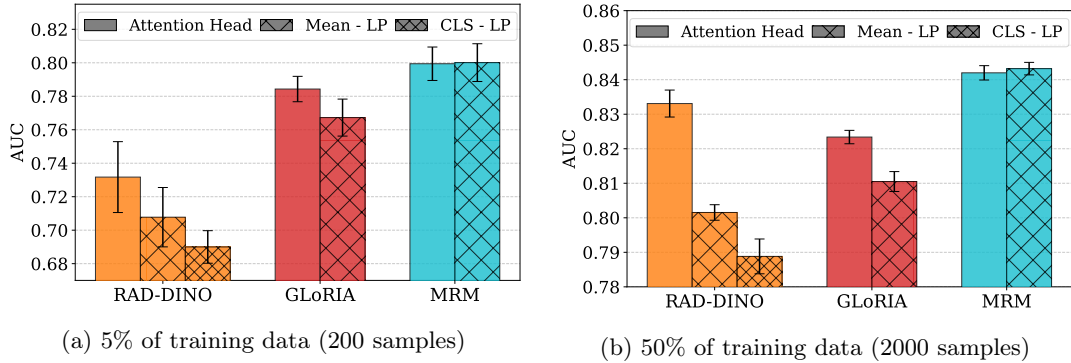


Figure 16: **MIMIC 5x1200** - Ablation of different fine-tuning heads on the image-only model. "Attention Head" is the self-attention head used in all experiments in the main paper, "Mean - LP" is mean-pooling followed by linear probing, and "CLS - LP" uses linear probing on the CLS token embedding.

C.2 Temperature parameter

We perform an ablation experiment on the temperature parameter (τ) in Equation 2 on **Readmission** (Figure 17) and **MIMIC 5x1200** (Figure 18). The distillation models consistently outperform the image-only baseline, regardless of temperature, on the **Readmission** dataset. On **MIMIC 5x1200**, the choice of τ seems to have a modest impact (except for RAD-DINO in Figure 18a).

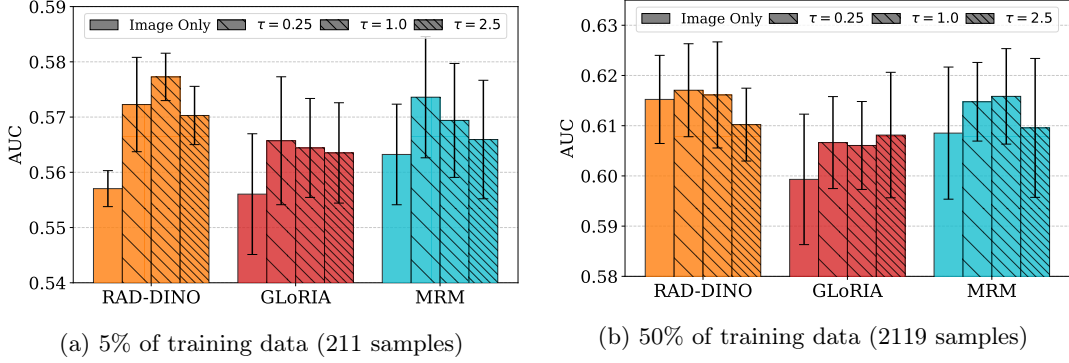


Figure 17: **Readmission** - Distillation performance with different temperatures τ .

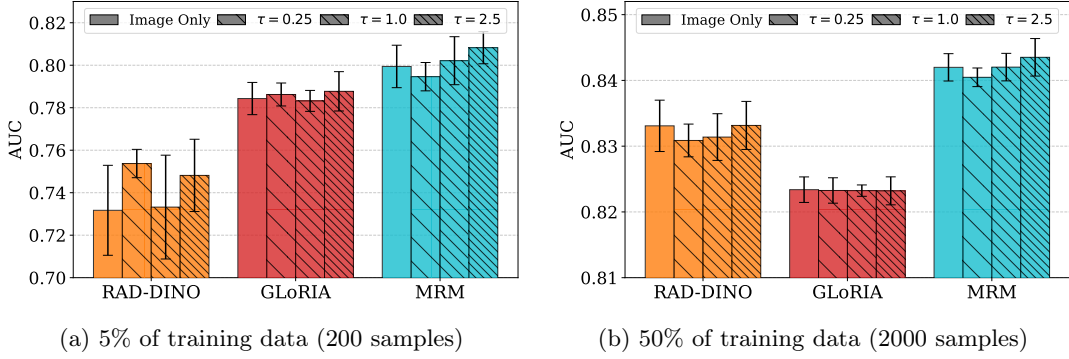


Figure 18: **MIMIC 5x1200** - Distillation performance with different temperatures τ .

C.3 Choice of text model

To evaluate the impact of the text model in our distillation setup, we train two additional teacher models that each use a different BERT encoder. Apart from the BioViL-T, we use CXR-BERT-general (Boecking et al., 2022), trained with radiology reports, but without the image-based fine-tuning of BioViL-T. We further include Bio_ClinicalBERT (Alsentzer et al., 2019), which has been trained on clinical notes from MIMIC-III, but not radiology reports. Figures 19 and 20 show the performance of the image-only students distilled from these teachers. The results demonstrate that while the choice of text model impacts distillation quality, benefits are observed for all three on the **Readmission** dataset. While it would be interesting to explore using the accompanying text encoders for the VLM backbones, not all of these are available, and we limit ourselves to the three covered here to make the comparison as fair as possible. CXR-BERT-general and Bio_ClinicalBERT are available on <https://huggingface.co/microsoft/BiomedVLP-CXR-BERT-general> and https://huggingface.co/emilyalsentzer/Bio_ClinicalBERT respectively.

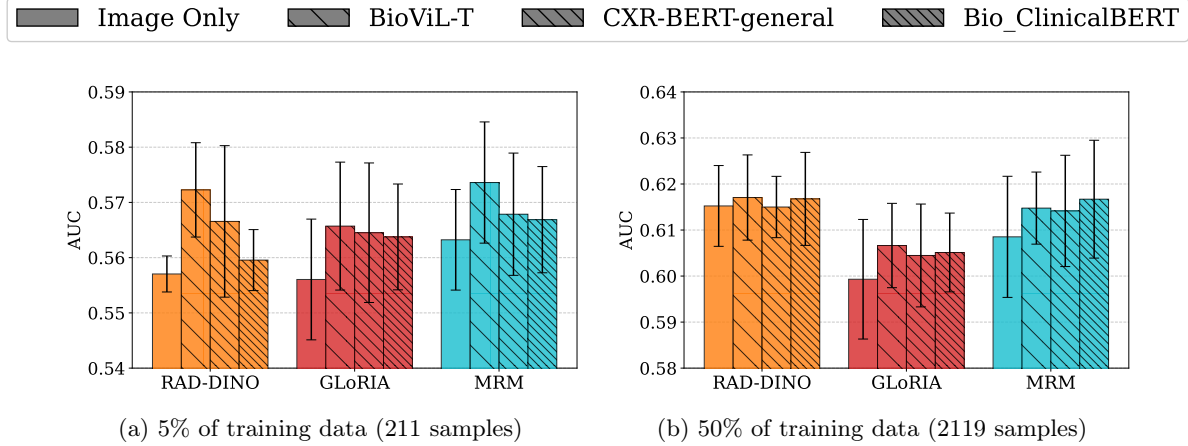


Figure 19: **Readmission** - Distillation from teachers trained with different text backbones.

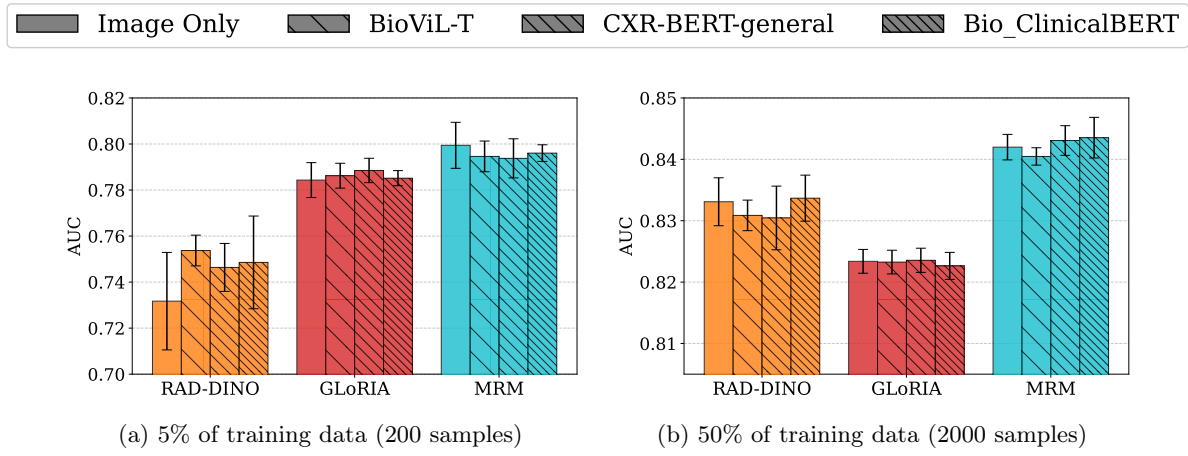


Figure 20: **MIMIC 5x1200** - Distillation from teachers trained with different text backbones.

D Compute

Experiments were primarily performed on the NVIDIA T4 (16GB) GPU. RAD-DINO had to be run on an NVIDIA A100 (40GB) to avoid memory constraints. No experiment ran for more than 8 hours, with the majority completing in less than half that time. Given this, we approximate that all experiments run in Figure 4 require less than 1,000 hours. Training of the additional teacher, distillation, and self-distillation models in Figure 5 meant that we had 4 methods for each of the 6 backbones over 5 seeds. Again using the upper limit of 8 hours per run, each subfigure in 5 took less than $8 \cdot 6 \cdot 4 \cdot 5 = 960$ hours to run.

E Dataset Licenses

MIMIC JPEG images and labels extracted from reports were collected from MIMIC-CXR-JPG 2.1.0 <https://physionet.org/content/mimic-cxr-jpg/2.1.0/>. Free-text reports and image metadata were fetched from MIMIC-CXR 2.1.0 <https://physionet.org/content/mimic-cxr/2.1.0/>. Patient admission information (used for the **3-Day Discharge** dataset) was gathered from MIMIC-IV 3.1 <https://physionet.org/content/mimiciv/3.1/>. All data is provided under the PhysioNet Credentialed Health Data License 1.5.0 <https://physionet.org/content/mimic-cxr/view-license/2.1.0/>.

INSPECT The INSPECT dataset was downloaded from <https://stanfordaimi.azurewebsites.net/datasets/318f3464-c4b6-4006-9856-6f48ba40ad67>. The data is licensed under the Stanford University Dataset Research Use Agreement, provided on the same page.